ARMY RESEARCH LABORATORY

Deformation Mechanisms and High Strain Rate Properties of Magnesium (Mg) and Mg Alloys

by Bin Li, Logan Shannahan, Evan Ma, Kaliatt T. Ramesh, Suveen Mathaudhu, Robert J. Dowding, and James W. McCauley

ARL-TR-6085   **August 2012**

NOTICES

Disclaimers

The findings in this report are not to be construed as an official Department of the Army position unless so designated by other authorized documents.

Citation of manufacturer's or trade names does not constitute an official endorsement or approval of the use thereof.

Destroy this report when it is no longer needed. Do not return it to the originator.

Army Research Laboratory

Aberdeen Proving Ground, MD 21005-5066

Deformation Mechanisms and High Strain Rate Properties of Magnesium (Mg) and Mg Alloys

Bin Li, Logan Shannahan, Evan Ma, and Kaliatt T. Ramesh
Johns Hopkins University

Suveen Mathaudhu, Robert J. Dowding, and James W. McCauley
Weapons and Materials Research Directorate, ARL

---

1. REPORT DATE *(DD-MM-YYYY)*	2. REPORT TYPE	3. DATES COVERED (From - To)
August 2012	Final	October 2005–September 2011

4. TITLE AND SUBTITLE	5a. CONTRACT NUMBER
Deformation Mechanisms and High Strain Rate Properties of Magnesium (Mg) and Mg Alloys	W911NF-06-2-0006
	5b. GRANT NUMBER
	5c. PROGRAM ELEMENT NUMBER

6. AUTHOR(S)	5d. PROJECT NUMBER
Bin Li,* Logan Shannahan,* Evan Ma,* Kaliatt T. Ramesh, *Suveen Mathaudhu, Robert J. Dowding, and James W. McCauley	BH64
	5e. TASK NUMBER
	5f. WORK UNIT NUMBER

7. PERFORMING ORGANIZATION NAME(S) AND ADDRESS(ES)	8. PERFORMING ORGANIZATION REPORT NUMBER
U.S. Army Research Laboratory ATTN: RDRL-WM Aberdeen Proving Ground, MD 21005-5066	ARL-TR-6085

9. SPONSORING/MONITORING AGENCY NAME(S) AND ADDRESS(ES)	10. SPONSOR/MONITOR'S ACRONYM(S)
	11. SPONSOR/MONITOR'S REPORT NUMBER(S)

12. DISTRIBUTION/AVAILABILITY STATEMENT

Approved for public release; distribution is unlimited.

13. SUPPLEMENTARY NOTES

*Johns Hopkins University, Baltimore, MD 21218

14. ABSTRACT

This report summarizes research at the Johns Hopkins University Center for Advanced Metallic and Ceramic Systems on lightweight magnesium (Mg) and Mg alloys, under the sponsorship of the U.S. Army Research Laboratory (ARL) Materials Center of Excellence (MCOE) during 2007–2010. In collaboration with ARL, extensive studies have been conducted on the fundamental deformation mechanisms of pure Mg and the mechanical properties at high strain rate of ultrafine-grained Mg alloys. Atomistic simulations, transmission electron microscopy, and Kolsky bar testing have been performed to investigate the deformation mechanisms of Mg and Mg alloys. Newly uncovered mechanisms of pyramidal slip, $\{10\bar{1}1\} < 10\bar{1}2 >$ twinning and $\{10\bar{1}2\} < 10\bar{1}1 >$ twinning, were observed for hexagonal close-packed Mg. High strain rate properties of Mg alloys with submicron grain sizes were also studied.

15. SUBJECT TERMS

magnesium, deformation mechanisms, high strain rate, twinning, zonal dislocations

16. SECURITY CLASSIFICATION OF:			17. LIMITATION OF ABSTRACT	18. NUMBER OF PAGES	19a. NAME OF RESPONSIBLE PERSON James W. McCauley
a. REPORT	b. ABSTRACT	c. THIS PAGE			19b. TELEPHONE NUMBER *(Include area code)*
Unclassified	Unclassified	Unclassified	UU	26	410-306-0711

Contents

List of Figures

Acknowledgments

1. Introduction

Magnesium (Mg) and Mg alloys are desirable structural materials for lightweight systems due to their very low density (~1740 kg/m^3, 34% less than Al). In recent years, attention has been focused on the need for significant improvements in mechanical properties to enable more widespread application of these materials. This increased interest led to the organization of an international workshop at Johns Hopkins University during 1–2 May 2007 (*1*) and a Sagamore conference in June 2010 (*2*). A comprehensive historical review of the U.S. military applications of Mg alloys has recently been published (*3*). However, compared with metals that have higher symmetry crystal structures, the plastic deformation mechanisms in the hexagonal-close-packed (hcp) Mg are much more complicated and, consequently, were less understood (*4–8*). In Mg, three possible dislocation Burgers vectors can be operative on various slip planes (*7, 9*): $<a>=\frac{1}{3}<11\bar{2}0>$ (on basal or prismatic planes), $<c>=\frac{1}{3}<11\bar{2}0>$ (on prismatic planes), and $<c+a>=\frac{1}{3}<11\bar{2}\bar{3}>$ (on the $\{11\bar{2}2\}$ pyramidal plane). Since type *<a>* dislocations cannot accommodate the strain along the *<c>* axis, pyramidal slip is activated during plastic deformation. Due to the limited number of slip systems, twinning also plays an important role in the plastic deformation of Mg. The two dominant twinning modes in Mg are $\{10\bar{1}1\}<10\bar{1}\bar{2}>$ and $\{10\bar{1}2\}<10\bar{1}\bar{1}>$ (*10–14*), with the latter being the more commonly observed in deformed Mg and other hcp metals. The slip and twinning systems in Mg are summarized in figure 1.

The complicated deformation mechanisms (figure 1) have been extensively studied by simulation and experiment during the past few decades. However, the results have been controversial and inconclusive. For example, if we closely examine all the slip systems and the two twinning systems, an intriguing finding is that the pyramidal slip is not found on either of the two twin planes. Despite the fact that Mg does not twin on the $\{11\bar{2}2\}$ plane, it has always been claimed that there is a pyramidal *<c+a>* slip system $\{11\bar{2}2\}<11\bar{2}\bar{3}>$ on this plane (*4–8*).

The twinning mechanisms in the lower symmetry hcp structure have remained unsolved because twinning in Mg involves complicated processes, including a homogeneous shear and local atomic shuffling. The Burgers vectors of the twinning dislocations are only a small fraction of the twinning direction vector η_1, distinctive from the twinning process in face-centered-cubic structures where simple shear alone, via a Shockley partial dislocation, can accomplish the twinning (*15–20*). Exactly what happens at the twin/matrix interfaces has remained obscure, despite the efforts over the past several decades.

To enable potential applications in extreme dynamic environments, mechanical properties at high strain rates under dynamic testing must also be studied. The goals of this research project have been to: (1) resolve the mechanisms of dislocation slip and twinning in Mg, particularly the
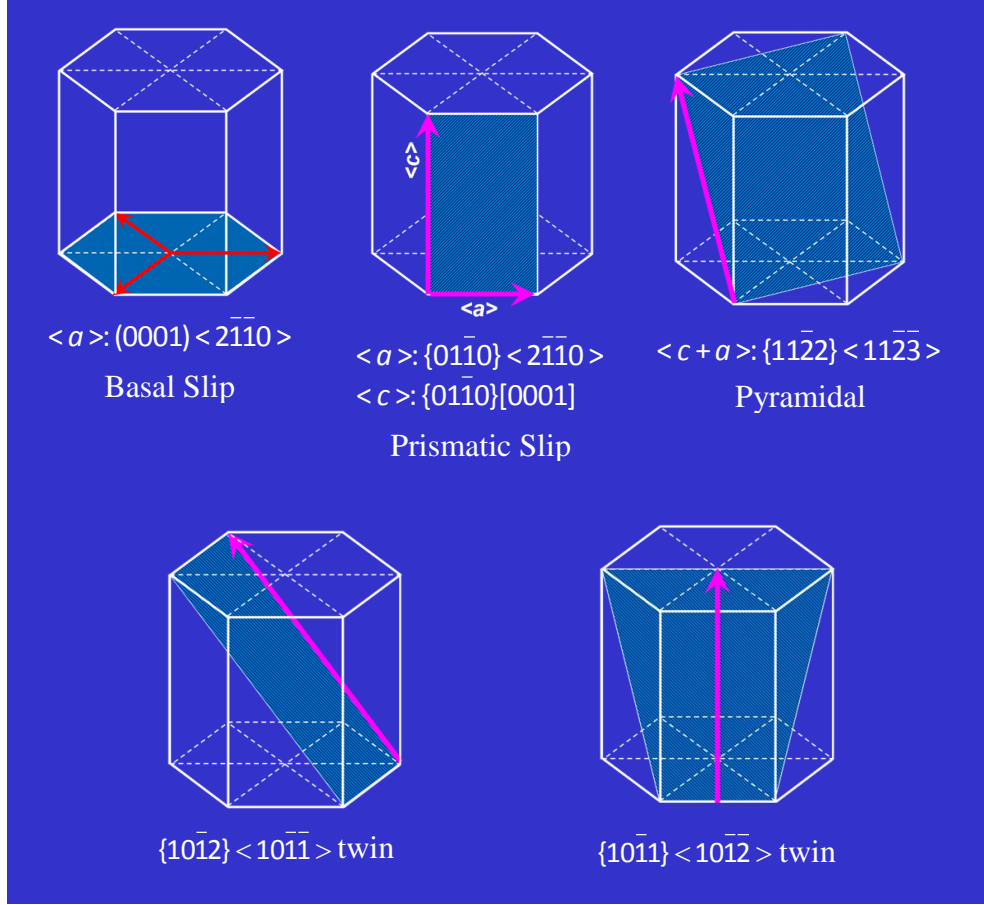
Figure 1. Schematic of the slip and twinning systems in hexagonal close-packed (hcp) Mg. Note that the pyramidal slip is on neither of the two twinning planes.

pyramidal slip and the interfacial dynamics at the twin boundaries (TBs) (the results obtained can be extended to other hcp metals, such as Ti, Zr, Co, etc.), (2) improve the mechanical properties through grain refining techniques such as severe plastic deformation (SPD) processing, and (3) study high strain rate properties of the ultrafine-grained (UFG) Mg and Mg alloys.

2. Methodology

Molecular dynamics (MD) simulations and the embedded atom method (EAM) interatomic potential for Mg developed by Liu et al. (*21*) were utilized to study dislocation slip and twinning in Mg. The EAM potential was fit not only to experimental data but also force data obtained from *ab initio* calculations using local orbital pseudopotentials based on the local density approximation in the density functional theory. We validated the EAM potentials by calculating the stacking fault energy and the split distance between the Shockley partial dislocations (*22–24*), and the results obtained were satisfactory.

We used transmission electron microscopy (TEM) to observe pyramidal dislocations, stacking faults, and twinning dislocations at the TBs. TEM specimens were polished using a Tenupol-3 electropolisher with a perchloric (<2%) ethanol solution. The specimens were then cleaned by ion milling for ~0.5 h with liquid nitrogen cooling and using very gentle milling conditions (low incidental angle and low voltage). TEM microstructural analyses were carried out on a Philips 420 microscope with a double-tilt specimen stage. The accelerating voltage was 120 kV. We also performed high-resolution electron microscopy on an FEI CM 300 microscope.

UFG samples were prepared by equal-channel, angular-extrusion (ECAE) processing. In this method, a sample is pressed through a die having intersecting channels of equal size and shape, often at right angles. Large shear strain is imparted to the sample, while the cross section of the sample is maintained during processing. Fine grains result due to dynamic recovery and recrystallization. This processing method has been successful in processing a wide range of metallic materials with refined grain structures.

Compression Kolsky bar (also known as the split-Hopkinson pressure bar) experiments were conducted to obtain the mechanical response at high strain rates ($>10^3$ s^{-1}). The test specimens had a square cross section of 4×4 mm, with a height-to-width ratio ~0.6. The interfaces between the specimens and the bars were lubricated with grease. A digital high-speed camera (DRS Hadland Ultra 8), with the ability to record eight frames at a rate of 10^8 frames per second, was synchronized with the Kolsky bar system to record the deformation and failure of the specimens in dynamic loading. The cuboidal specimens were polished on one rectangular surface to a mirror-like finish. This surface was oriented toward the high-speed camera.

3. Results and Discussions

3.1 Pyramidal Slip on {10$\bar{1}$1} Twinning Plane

Figure 2 shows the basal planes colored alternately red and green. Only a portion of the crystal is shown, with part of a created cavity at the lower right corner serving as a nucleation site for dislocations. The two-dimensional atomic figure is a projection of the three-dimensional structure such that each column of atoms corresponds to a basal plane.

Under uniaxial tension along the <c> axis, dislocation slip occurs on a pyramidal plane. A dislocation (inside the circle) can be seen to nucleate from the cavity and glides toward the free surface. The slip plane, which is inclined with respect to the basal planes, is identified as $(0\bar{1}11)$ (the trace of the slip plane is shown as a broken blue line). The Burgers vector of the dislocation has a magnitude of $\frac{1}{2} \times \frac{1}{2}[01\bar{1}2]$. As shown in figure 2, a change in the stacking sequence in the region behind the dislocation core can clearly be seen. Each basal plane in the nonsheared
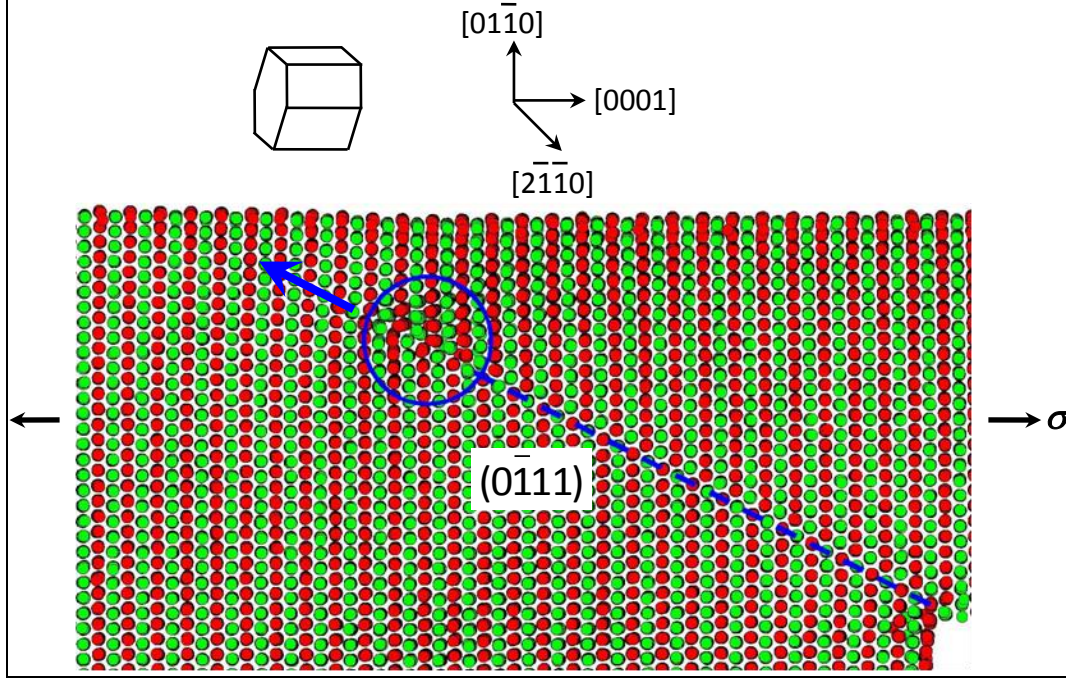
Figure 2. A dislocation (circled region) is nucleated at the lower right corner and propagates towards the free surface (indicated by the arrow). The trace of the slip plane is marked with a broken blue line. The slip plane is identified as (01̄11). The dislocation creates a stacking fault behind. Note the change in color for each of the basal planes after the dislocation propagates through.

region remains single colored, while those in the sheared region become mixed, indicating a stacking fault is created by the pyramidal dislocation (*25*). Figure 3 shows well-defined dark/bright fringes typical of stacking faults observed in TEM. We believe that this is the first TEM observation of wide stacking faults in Mg and other hcp metals.

The simulation results and the TEM observations demonstrate the following: (1) the slip plane of pyramidal dislocations is not the previously claimed $\{1\bar{1}22\}$ but $\{10\bar{1}1\}$, one of the twinning planes; and (2) unit pyramidal dislocations $\{1\bar{1}22\}<11\bar{2}\bar{3}>$ do not exist in Mg and other hcp metals, contrary to previous reports.

3.2   Zonal Dislocations Promoting $\{10\bar{1}1\}<10\bar{1}\bar{2}>$ Twinning

The critical issue associated with deformation twinning in hcp metals is which twinning dislocations can promote twin growth under an external load. It was realized that the twinning dislocations have to be "zonal dislocations" comprising multiple twinning planes (*26*). In addition, atomic shuffling is required to establish the correct twin orientation relationship. The role of shuffling in twinning has been overlooked in previous research.
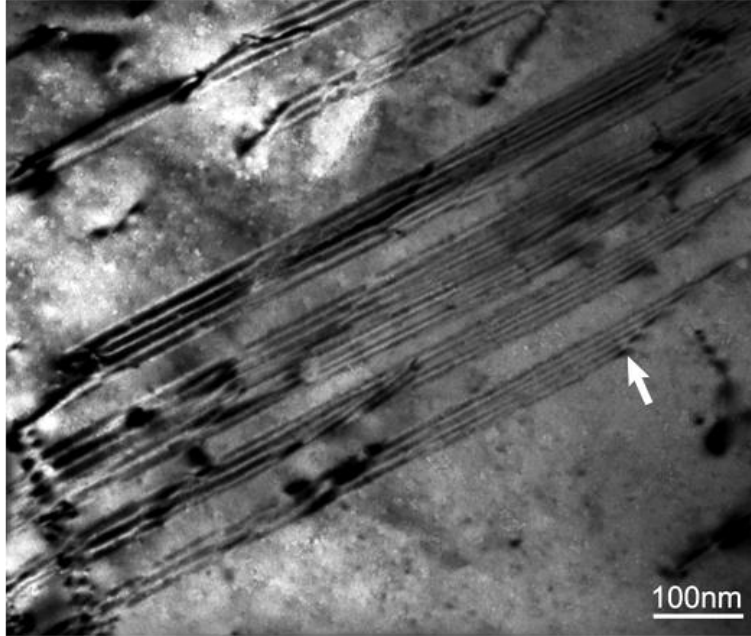
Figure 3. Well-defined fringes from stacking faults in a commercially pure Mg sample uniaxially compressed to 10%. The associated dislocations (indicated by the arrow) can be clearly seen, which are presumably emitted from a low-angle grain boundary (lower left).

In figure 4, a single crystal was loaded in tension perpendicular to the $<c>$ axis, and $\{10\bar{1}1\}<10\bar{1}\bar{2}>$ twinning is observed. The TBs are marked with white bold lines. Multiple steps at the TBs are the traces of the twinning dislocations (indicated by the arrows). The twinning plane can be identified as $\{10\bar{1}1\}$. This twinning mode causes contraction along the $<c>$ axis.
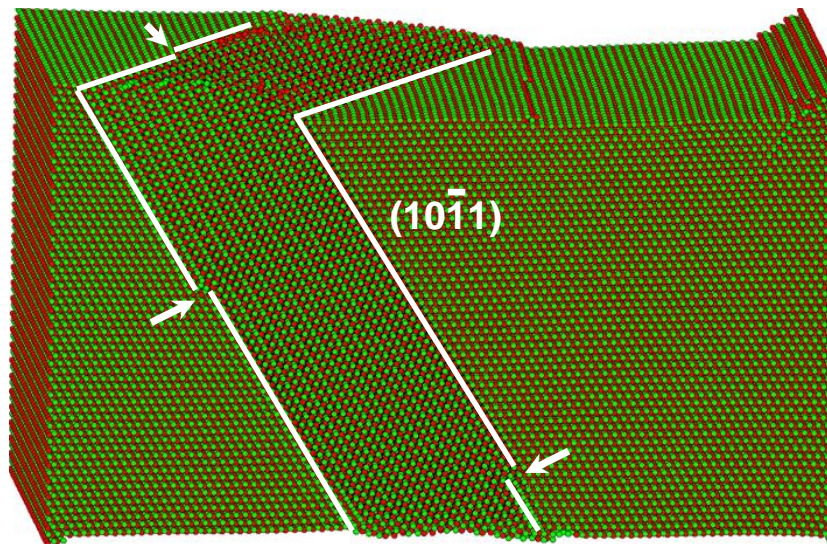
Figure 4. Three-dimensional view of the twin and the matrix. The two interfaces are marked with bold white lines. The twinning plane can be identified as $(10\bar{1}1)$. Steps on the twin boundaries can be seen (indicated by arrows).

5

Figure 5 shows a single crystal that has undergone twinning during deformation. Atoms that have a coordination number other than 12 are plotted as red circles, and other atoms with a coordination number equal to 12 are shown as little blue dots. Atoms residing in the dislocation core and at the twin/matrix interfaces are highlighted and tracked during simulation. It can be clearly seen that twinning dislocations nucleate at the intersection of the twinning plane and the top surface and glide downwards, leading to twin growth (thickening) (*27*).
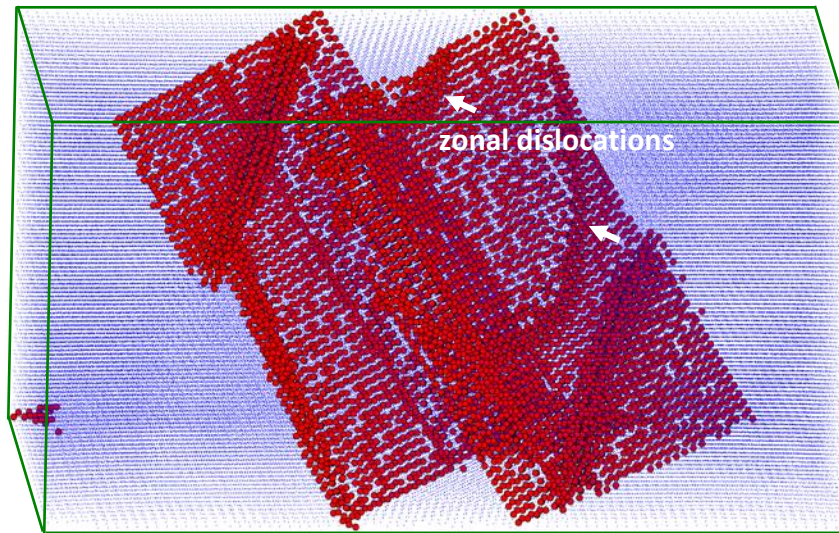
Figure 5. Zonal twinning dislocations were observed at the TBs (indicated by the arrows). The plot was made such that the atoms at the twin boundaries are highlighted in red, while other atoms were plotted as little blue dots. The core of the zonal dislocations spreads over two twinning planes.

Our TEM analysis confirms that the $\{10\bar{1}1\} < 10\bar{1}\bar{2} >$ twinning is indeed promoted by the twinning dislocations at the TBs (*28*). In figure 6, the dark/bright fringes parallel to the TBs are the contrast from the twin/matrix interfaces. It can be seen that twinning dislocations (indicated by the thin arrows) are confined inside the TBs, which are also the interfacial dislocations. It can also be seen that matrix dislocations (indicated by the block arrows) have similar diffraction contrast as the twinning dislocations, indicating that these dislocations have the same Burgers vector component along the twinning direction.
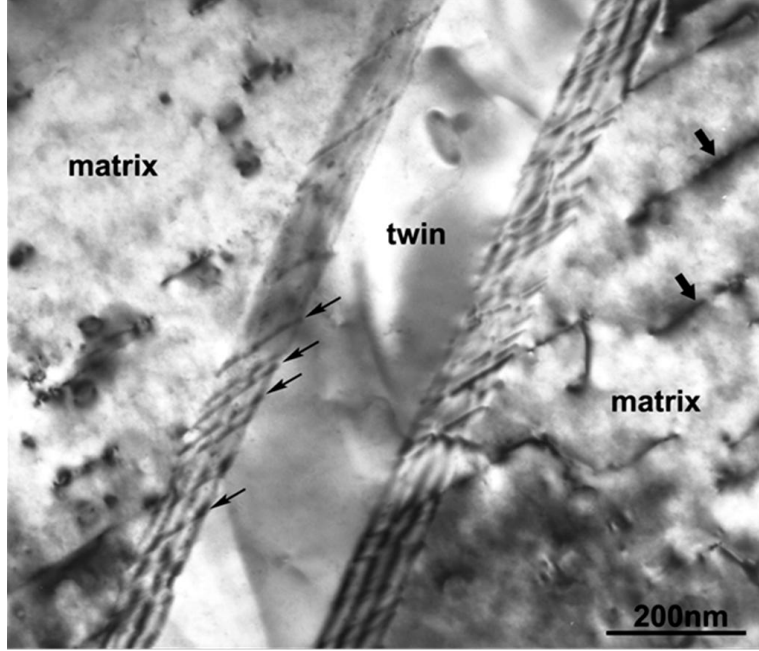
Figure 6. TEM observation of twinning dislocations (indicated by the thin arrows) confined in the twin boundary, and matrix pyramidal dislocations (indicated by the block arrows). Note that the twinning dislocations and the pyramidal dislocations have similar diffraction contrast, indicating that pyramidal slip must be on the twinning plane.

3.3 Atomic Shuffling Dominated $\{10\bar{1}2\}<10\bar{1}\bar{1}>$ Twinning

In the $\{10\bar{1}1\}<10\bar{1}\bar{2}>$ twinning mode, a zonal twinning dislocation can be well defined, and atoms at the TBs slightly shuffle off-plane to create a twin. However, the scenario of the most commonly observed $\{10\bar{1}2\}<10\bar{1}1>$ twinning mode in Mg and other hcp metals is very different. The calculated Burgers vector of the "twinning dislocation" is only 0.024 nm, about 1/31 of the twining direction vector η_1. The dislocations that promote twin growth have been controversial for decades.

A new crystallographic model (*29*) has been proposed to describe the $\{10\bar{1}2\}<10\bar{1}\bar{1}>$ twinning. This model only involves local atomic shuffling to accomplish the twinning process with little twinning shear. Figure 7 schematically shows our twinning model. The parent hcp lattice cell is illustrated with atoms in a red/blue/red color scheme to show the *ABABAB* stacking sequence, and the basal planes are marked as *A* (red) and *B* (pink), perpendicular to the paper plane and stacking from the bottom up. If those atoms with distances close to a_0 (the lattice parameter) are connected, it can immediately be seen that a new "hcp" lattice can be constructed with a misorientation ~90° with respect to the original basal plane. Note that this misorientation satisfies the $\{10\bar{1}2\}$ twin relationship, and it easily seen that the $\{10\bar{1}2\}$ plane is common to both lattices. The new "basal" planes are marked by *A′* (dark green) and *B′* (light green), parallel to
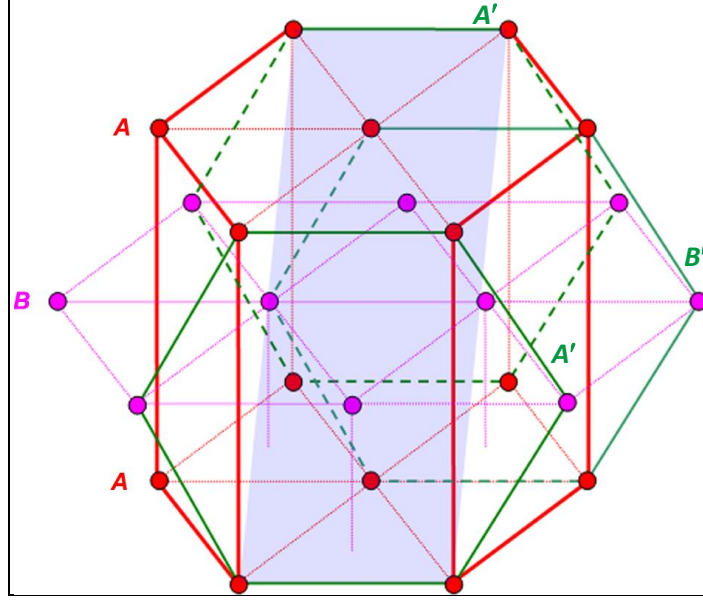
Figure 7. Schematic of constructing a new hcp lattice (dark blue; the basal planes are parallel to the paper plane) from an existing hcp lattice (red; the basal planes are perpendicular to the paper plane). The stacking of the parent basal planes is marked as *ABABAB...* (*B* layer in pink), whereas the stacking of the new basal planes is marked as *A'B'A'B'A'B'*. The two lattices share a common $\{10\bar{1}2\}$ plane and, hence, they satisfy the twin relationship. Local shuffling is required to correct the distortion in the new hcp lattice so the correct stacking sequence and c/a ratio can be established.

the paper plane and marked as *A'B'A'B'A'B*. However, the new lattice is distorted and does not have the correct hcp stacking sequence yet. This is obvious since the prism planes of an hcp lattice are double-layered, but the constructed prism plane is flat. Conversely, the constructed basal planes are double-layered instead of flat, as is expected. To correct these distortions, the pink atoms of the new basal (the *A'* plane) have to shuffle outwards by $\frac{\sqrt{3}}{6}a_0$ (~0.092 nm for Mg and ~0.085 nm for Ti) to make the new basal flat, while the atoms of the *B'* plane have to shuffle downwards by $\frac{\sqrt{3}}{6}a_0$ to make the new prism double-layered. These shuffles, plus other minor adjustments to reach the correct *c/a* ratio, with magnitudes much shorter than any existing dislocation Burgers vectors, exactly convert the parent basal planes to the twin prism planes and the parent prism planes to the twin basal planes. As can be seen, this reconstruction process involves no definable dislocation but only local shuffling.

Our model explains the reasons why: (1) $\{10\bar{1}2\}<10\bar{1}\bar{1}>$ twinning is reversible, and (2) hcp metals have a natural tendency to reorient the basal plane parallel to the loading axis (i.e., texturing) during plastic deformation.

3.4 High Strain Rate Properties of UFG Mg Alloys

The microstructure of the UFG sample (AZ31B) processed by seven ECAE passes is shown in figure 8. The grain structure is significantly refined, with an average grain size of about 250 nm. To the best of our knowledge, this is the finest Mg alloy grain size obtained by ECAE processing; the grain boundaries are observed to be high-angle grain boundaries.
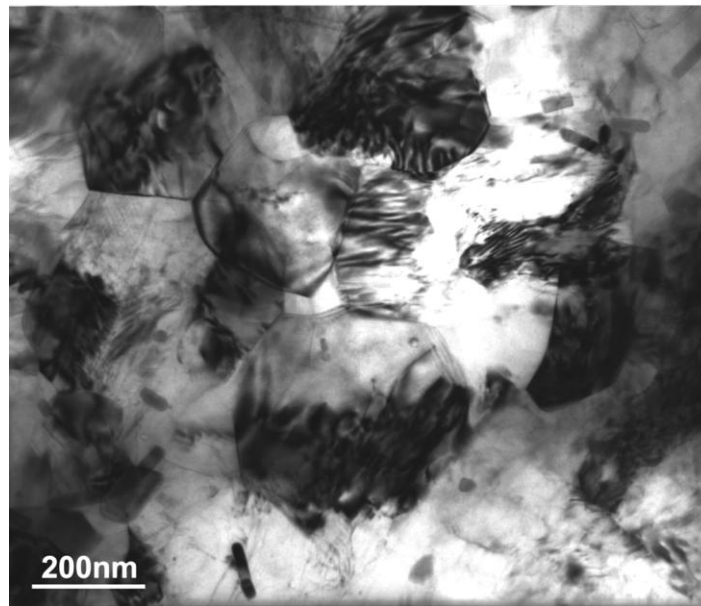
Figure 8. Ultrafine-grained (UFG) AZ31B samples were obtained by ECAE processing. The TEM micrograph shows the average grain size is about 250 nm.

In figure 9, the stress-strain curves at high strain rates (~4500 s^{-1}) of the samples with various ECAE processing is presented. As the number of passes increases, the grain size decreases, with an expected increase in the elastic strength. Significant differences in the flow stresses can be seen between the coarse-grained samples and the UFG samples. For the coarse-grained samples, a large increase in work hardening can be seen, whereas the UFG samples harden only moderately. The difference in the plastic flow indicates a transition in the deformation mechanisms from twinning dominated flow in the coarse-grained samples to dislocation dominated flow in the UFG samples (*30*).
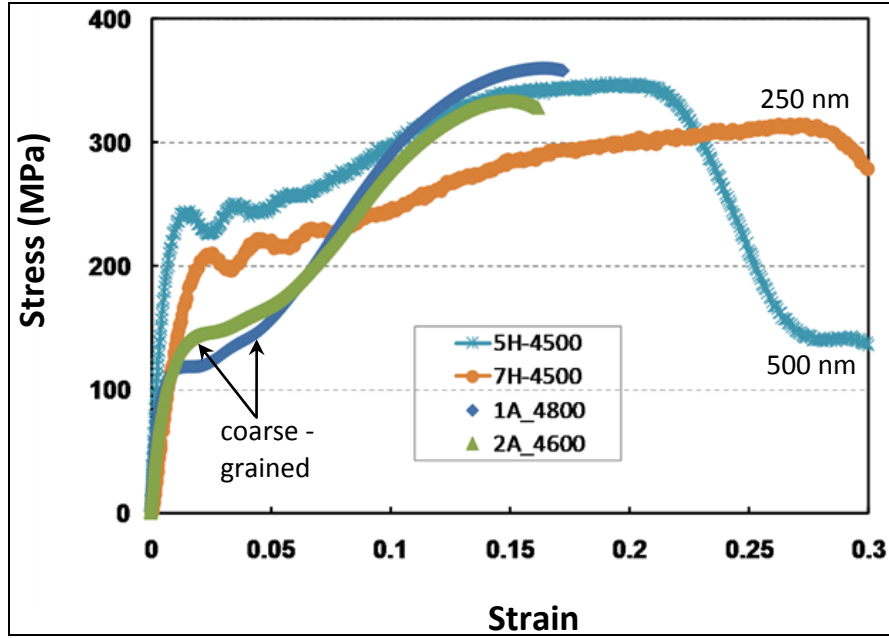
Figure 9. Mechanical properties of an AZ31B Mg alloy at high strain rates
(~4500 s^{-1}) processed by different number of ECAE passes (1A – 1
pass; 2A – 2 passes 5H – 5 passes; 7H – 7 passes). The grain size
decreases as the number of passes increases. In general, the elastic
strength increases as the grain size decreases. A drastic increase in
work hardening can be seen in coarse-grained samples, a sharp contrast
to only moderate hardening in UFG samples; this indicates a transition
in deformation mechanism.

In figure 10, high strain rate mechanical test data for a number of Mg alloys in the literature
(*30–35*) are presented in the form of a semi-log plot. All of the data are taken from the extrusion
direction. It is observed that the compressive strength increases as the strain rate increases,
indicating a rate dependence of the mechanical properties of Mg alloys. Note that figure 7 only
provides a general sense of the mechanical properties of Mg alloys at high strain rates. Direct
comparison of the properties must be done with caution since the mechanical properties strongly
depend upon the processing history, sample orientation, and microstructure.
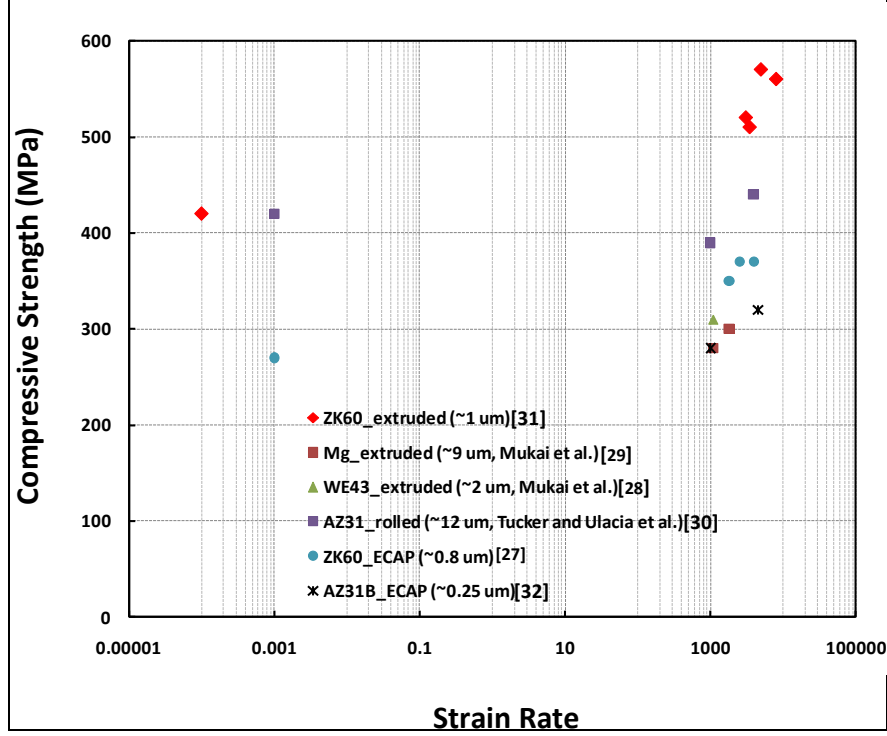
Figure 10. A summary of compressive strengths of Mg alloys tested at high strain rates (>1000 s^{-1}); quasi-static data are also included. All data points are from the extrusion direction. Note: this plot only provides a general sense of the mechanical properties at dynamic range of Mg alloys. Direct comparison in mechanical properties of Mg alloys must be done with caution because the experimental results strongly depend upon processing history, sample orientation, and microstructure.

4. Conclusions

1. Atomistic simulations and the TEM analysis demonstrates that pyramidal slip in Mg and other hcp metals is not on the often-claimed $\{11\bar{2}2\}$ plane, and the existence of $\{11\bar{2}2\}<11\bar{2}\bar{3}>$ pyramidal dislocations is questionable. Our results show that pyramidal slip occurs on the $\{10\bar{1}1\}$ plane, which is also a twinning plane, in Mg, with a Burgers vector $\frac{1}{2}\times\frac{1}{2}<10\bar{1}\bar{2}>$ along the twinning direction. This incomplete dislocation creates a wide stacking fault on the $\{10\bar{1}1\}$ plane, as confirmed by TEM analysis.

11

2. MD simulations show that the $\{10\bar{1}1\} < 10\bar{1}\bar{2} >$ twinning is promoted by a zonal dislocation, with the dislocation core spreading over two twinning planes. The overall Burgers vector adds up to $\frac{1}{2} \times \frac{1}{2} < 10\bar{1}\bar{2} >,$ which equals a pyramidal dislocation in the matrix.

3. A new crystallographic model has been proposed to describe the most commonly observed $\{10\bar{1}2\} < 10\bar{1}\bar{1} >$ twinning in Mg and other hcp metals. In this model, a new "hcp" lattice can be reconstructed from the existing matrix lattice, with the $<c>$ axes of the two lattices nearly perpendicular to each other, satisfying the twin orientation relationship. Minoratomic shuffling is required to accomplish the correct hcp stacking in the new lattice. The magnitude of the shuffling is much shorter than any Burgers vector of matrix dislocations but much larger than the calculated twinning Burgers vector, indicating that the $\{10\bar{1}2\} < 10\bar{1}\bar{1} >$ twinning mode is shuffling dominated.

5. References

1. Ma, E.; Ramesh, K. T.; Dowding, R.; McCauley, J. W. *International Magnesium Workshop*; ARL-SR-162; U.S. Army Research Laboratory: Aberdeen Proving Ground, MD, July 2008.

2. Mathaudhu, S.; Dowding, R.; McCauley, J. W. *47th Sagamore Army Materials Research Conference on Advances in Lightweight Structural Materials*, St. Michaels, MD, 14–17 June 2010.

3. Mathaudhu, S.; Nyberg, E. A. *Magnesium Technology 2010;* Agnew, S. R. et al., Eds.; TMS; 2010; pp 27–33.

4. Yoshinaga, H.; Horiuchi, R. *Trans. JIM* **1963**, *4*, 1.

5. Obara, T.; Yoshinaga, H.; Morozumi, S. *Acta Metall.* **1973**, *21*, 845.

6. Stohr, J. F.; Poirier, J. P. *Phil. Mag.* **1972**, *25*, 1313.

7. Yoo, M. H.; Morris, J. R.; Ho, K. M.; Agnew, S. R. *Metall. Trans. A* **2002**, *33A*, 813.

8. Koike, J.; Kobayahsi, T.; Mukai, T.; Watanabe, H.; Suzuki, M.; Maruyama, K.; Higashi, K. *Acta Mater.* **2003**, *51*, 2055.

9. Bacon, D. J.; Vitek, V. *Metall. Trans. A* **2002**, *33A*, 721.

10. Serra, A.; Bacon, D. J. *Phil. Mag. A* **1996**, *73*, 333.

11. Serra, A.; Bacon, D. J. *Phil. Mag. A* **1996**, *63*, 1059.

12. Kucherov, L.; Tadmor, E. B. *Acta Mater.* **2007**, *55*, 2065.

13. Serra, A.; Bacon, D. J.; Pond, R. C. *Acta Metall.* **1988**, *36*, 3183.

14. Serra, A.; Pond, R. C.; Bacon, D. J. *Acta Metall. Mater.* **1991**, *39*, 1469.

15. Minonishi, Y.; Ishioka, S.; Morozumi, S.; Koiwa, M.; Yamaguchi, M. *Philo. Mag. A* **1982**, *43*, 761.

16. Liang, M. H.; Bacon, D. J. *Phil. Mag. A* **1986**, *53*, 163.

17. Minonishi, Y.; Ishioka, S.; Morozumi, S.; Koiwa, M.; Yamaguchi, M. *Phil. Mag. A* **1981**, *43*, 1017.

18. Morris, J. R.; Scharff, J.; Ho, K. M.; Turner, D. E. *Phil. Mag. A* **1997**, *76*, 1065.

19. Humakura, H.; Minonishi, Y.; Koiwa, M. *Phil. Mag. A*, **1990**, *62*, 525.

20. Agnew, S. R.; Horton, J. A.; Yoo, M. H. *Metall. Trans. A* **2002**, *33A*, 851.

21. Liu, X. Y.; Adams, J. B.; Erocolessi, F.; Moriarty, J. A. *Modelling Simul. Mater. Sci. Eng.* **1996**, *4*, 293.

22. Fleischer, R. L. *Scripta Met*. **1986**, *20*, 223.

23. Chetty, N.; Weinert, M. *Phys. Rev. B* **1997**, *56*, 55.

24. Gotsis, H. J.; Papaconstantopoulos, D. A.; Mehl, M. J. *Phys. Rev. B* **2002**, *65*, 134101.

25. Li, B.; Ma, E. *Philo. Mag.* **2009**, *89*, 1223.

26. Christian, J. W.; Mahajan, S. *Prog. Mater. Sci.* **1995**, *39*, 1.

27. Li, B.; Ma, E. *Acta Mater.* **2009**, *57*, 1734.

28. Li, B.; Yan, P. F.; Sui, S. L.; Ma, E. *Acta Mater.* **2010**, *58*, 173.

29. Li, B.; Ma, E. *Phys. Rev. Lett.* **2009**, *103*, 035503.

30. Li, B.; Joshi, S.; Azevedo, K.; Ma, E.; Ramesh, K. T.; Figueiredo, R. B.; Langdon, T. G. *Mater. Sci. Eng. A* **2009**, *517*, 24.

31. Mukai, T.; Mohri, T.; Mabuchi, M.; Nakamura, M.; Ishikawa, K.; Higashi, K. *Scripta Mater.* **1998**, 39, 1249.

32. Mukai, T.; Yamanoi, M.; Watanabe, H.; Ishikawa, K.; Higashi, K. *Mater. Trans. JIM* **2001**, *42*, 1177.

33. Tucker, M. T.; Horstemeyer, M. F.; Gullett, P. M.; El Kadiri, H.; Whittington, W. R. *Scripta Mater.* **2009**, *60*, 182.

34. Li, B.; Joshi, S. P.; Almagri, O.; Ma, Q.; Ramesh, K. T.; Mukai, T. *Acta Mater.* **2012**, *60*, 1818.

35. Li, B.; Mathaudu, S. N.; Shannahan, L.; Ramesh, K. T. In preparation.

NO. OF
COPIES ORGANIZATION

 1   DEFENSE TECHNICAL
(PDF   INFORMATION CTR
only)   DTIC OCA
        8725 JOHN J KINGMAN RD
        STE 0944
        FORT BELVOIR VA 22060-6218

 1   DIRECTOR
        US ARMY RESEARCH LAB
        IMAL HRA
        2800 POWDER MILL RD
        ADELPHI MD 20783-1197

 1   DIRECTOR
        US ARMY RESEARCH LAB
        RDRL CIO LL
        2800 POWDER MILL RD
        ADELPHI MD 20783-1197

NO. OF		NO. OF	
COPIES	ORGANIZATION	COPIES	ORGANIZATION

<table>
<tr><td>1</td><td>PEO GCS
SFAE GCS BCT/MS 325
M RYZYI
6501 ELEVEN MILE RD
WARREN MI 48397-5000</td><td>11</td><td>US ARMY TARDEC
AMSTRA TR R MS 263
K BISHNOI
D TEMPLETON (10 CPS)
WARREN MI 48397-5000</td></tr>
<tr><td>1</td><td>ABRAMS TESTING
SFAE GCSS W AB QT
J MORAN
6501 ELEVEN MILE RD
WARREN MI 48397-5000</td><td>1</td><td>COMMANDER
US ARMY RSRCH OFC
A RAJENDRAN
PO BOX 12211
RSRCH TRIANGLE PARK NC
27709-2211</td></tr>
<tr><td>1</td><td>COMMANDER
WATERVLIET ARSENAL
SMCWV QAE Q
B VANINA
BLDG 44
WATERVLIET NY 12189-4050</td><td>2</td><td>CALTECH
G RAVICHANDRAN
T AHRENS MS 252 21
1201 E CALIFORNIA BLVD
PASADENA CA 91125</td></tr>
<tr><td>1</td><td>COMMANDER
US ARMY AMCOM
AVIATION APPLIED TECH DIR
J SCHUCK
FT EUSTIS VA 23604-5577</td><td>5</td><td>SOUTHWEST RSRCH INST
C ANDERSON
K DANNEMANN
T HOLMQUIST
G JOHNSON
J WALKER
PO DRAWER 28510
SAN ANTONIO TX 78284</td></tr>
<tr><td>1</td><td>USA SBCCOM PM SOLDIER SPT
AMSSB PM RSS A
J CONNORS
KANSAS ST
NATICK MA 01760-5057</td><td>3</td><td>SRI INTERNATIONAL
D CURRAN
D SHOCKEY
R KLOOP
333 RAVENSWOOD AVE
MENLO PARK CA 94025 21</td></tr>
<tr><td>1</td><td>UNIV OF DELAWARE
DEPT OF MECH ENGR
J GILLESPIE
NEWARK DE 19716</td><td>1</td><td>APPLIED RSRCH ASSOCIATES
D GRADY
4300 SAN MATEO BLVD NE
STE A220
ALBUQUERQUE NM 87110</td></tr>
<tr><td>3</td><td>AIR FORCE ARMAMENT LAB
AFATL DLJW
D BELK
J FOSTER
W COOK
EGLIN AFB FL 32542</td><td>1</td><td>INTERNATIONAL RSRCH
ASSOCIATES INC
D ORPHAL CAGE 06EXO
5274 BLACKBIRD DR
PLEASANTON CA 94566</td></tr>
<tr><td>1</td><td>TACOM ARDEC
AMSRD AAR AEE W
E BAKER
BLDG 3022
PICATINNY ARSENAL NJ
07806-5000</td><td>1</td><td>BOB SKAGGS CONSULTANT
S R SKAGGS
7 CAMINO DE LOS GARDUNOS
SANTA FE NM 87506</td></tr>
</table>

2	WASHINGTON ST UNIV INST OF SHOCK PHYSICS Y GUPTA J ASAY PULLMAN WA 99164-2814
1	COORS CERAMIC CO T RILEY 600 NINTH ST GOLDEN CO 80401
1	UNIV OF DAYTON RSRCH INST N BRAR 300 COLLEGE PARK MS SPC 1911 DAYTON OH 45469-0168
1	COMMANDER US ARMY TACOM AMSTA TR S L PROKURAT FRANKS WARREN MI 48397-5000
1	PM HBCT SFAE GCS HBCT S J ROWE MS 506 6501 11 MILE RD WARREN MI 48397-5000
3	COMMANDER US ARMY RSRCH OFC B LAMATINA D STEPP W MULLINS PO BOX 12211 RSRCH TRIANGLE PARK NC 27709-2211
1	NAVAL SURFACE WARFARE CTR CARDEROCK DIVISION R PETERSON CODE 28 9500 MACARTHUR BLVD WEST BETHESDA MD 20817-5700
2	LAWRENCE LIVERMORE NATL LAB R LANDINGHAM L369 J E REAUGH L282 PO BOX 808 LIVERMORE CA 94550

3	SANDIA NATL LAB J ASAY MS 0548 L CHHABILDAS MS 0821 D CRAWFORD ORG 0821 PO BOX 5800 ALBUQUERQUE NM 87185-0820
1	RUTGERS THE STATE UNIV OF NEW JERSEY DEPT OF CRMCS & MATLS ENGRNG R HABER 607 TAYLOR RD PICATINNY NJ 08854
1	THE UNIVERSITY OF TEXAS AT AUSTIN S BLESS IAT 3925 W BRAKER LN STE 400 AUSTIN TX 78759-5316
1	CERCOM R PALICKA 1960 WATSON WAY VISTA CA 92083
6	GDLS W BURKE MZ436 21 24 G CAMPBELL MZ436 30 44 D DEBUSSCHER MZ436 20 29 J ERIDON MZ436 21 24 W HERMAN MZ435 01 24 S PENTESCU MZ436 21 24 38500 MOUND RD STERLING HTS MI 48310-3200
1	JET PROPULSION LAB IMPACT PHYSICS GROUP M ADAMS 4800 OAK GROVE DR PASADENA CA 91109-8099
3	OGARA HESS & EISENHARDT G ALLEN D MALONE T RUSSELL 9113 LE SAINT DR FAIRFIELD OH 45014

NO. OF COPIES	ORGANIZATION
1	CERADYNE INC M NORMANDIA 3169 REDHILL AVE COSTA MESA CA 96626
2	JOHNS HOPKINS UNIV DEPT OF MECH ENGRNG K T RAMESH T W WRIGHT 3400 CHARLES ST BALTIMORE MD 21218
2	SIMULA INC V HORVATICH V KELSEY 10016 51ST ST PHOENIX AZ 85044
3	UNITED DEFENSE LP K STRITTMATTER E BRADY R JENKINS PO BOX 15512 YORK PA 17405-1512
10	NATL INST OF STANDARDS & TECH CRMCS DIV G QUINN STOP 852 GAITHERSBURG MD 20899
2	DIR USARL RDRL D C CHABALOWSKI V WEISS 2800 POWDER MILL RD ADELPHI MD 20783-1197 23

ABERDEEN PROVING GROUND

60	DIR USARL
	RDRL SL
	  R COATES
	RDRL WM
	  S KARNA
	  P BAKER
	  J MCCAULEY (10 CPS)
	RDRL WML
	  J NEWILL
	  M ZOLTOSKI
	RDRL WML B
	  D TAYLOR (10 CPS)
	RDRL WMM
	  R DOWDING

RDRL WMM A
  J SANDS
  T WEERASOORIYA
RDRL WMM D
  E CHIN
  K CHO
  G GAZONAS
  R SQUILLACIOTI
RDRL WMM E
  J LASALVIA
  P PATEL
RDRL WMM F
  J MONTGOMERY
RDRL WMP
  B BURNS
  S SCHOENFELD
RDRL WMP B
  C HOPPEL
  M SCHEIDLER
RDRL WMP C
  T BJERKE
  J CLAYTON
  D DANDEKAR
  M GREENFIELD
  S SEGLETES
  W WALTERS
RDRL WMP D
  T HAVEL
  M KEELE
  D KLEPONIS
  H MEYER
  J RUNYEON
RDRL WMP E
  P BARTKOWSKI
  M BURKINS
  W GOOCH
  D HACKBARTH
  E HORWATH
  T JONES
RDRL WML H
  T FARRAND
  L MAGNESS
  D SCHEFFLER
  R SUMMERS